VessComNet: Geometry-Aware 3D Vessel Completion Across Non-Contrast and Contrast-Enhanced CT Images

Linlin Yao[1⋆], Vivek Batheja[1], Praveen Thoppey Srinivasan Balamuralikrishna[1], Perry J. Pickhardt[2], Peter C. Grayson[3], Ronald M. Summers[1]

[1] Radiology and Imaging Sciences, National Institutes of Health Clinical Center, Bethesda, MD, USA
rms@nih.gov
[2] Department of Radiology, University of Wisconsin School of Medicine & Public Health, Madison, WI, USA
[3] National Institute of Arthritis and Musculoskeletal and Skin Diseases, National Institutes of Health,Bethesda, MD, USA

Abstract. Accurate vessel segmentation is essential for vascular disease assessment, yet automatic methods often produce fragmented and incomplete vessels due to low vessel-to-background contrast in non-contrast CT (NCCT) and curved vascular morphology in contrast-enhanced CT (CECT). To address this issue, we propose a geometry-aware 3D **Vess**el **Com**pletion **Net**work (**VessComNet**) that restores missing vessel segments in both NCCT and CECT. The framework leverages reliable CECT annotations to train a unified cross-protocol model, enabling vessel completion in challenging NCCT images without manual NCCT annotations. By incorporating centerline-guided geometric priors, the method preserves anatomical connectivity and structural plausibility. Experiments on three datasets demonstrate that our approach effectively restores missing regions and improves vessel continuity.

Keywords: 3D vessel completion · geometry-aware · non-contrast CT · contrast-enhanced CT.

1 Introduction

Vessel segmentation is a foundational task in medical imaging, crucial for diagnosing vascular diseases, planning interventions, and monitoring disease progression. Computed tomography (CT) serves as the primary imaging modality for this purpose due to its high spatial resolution. Two main protocols are used: contrast-enhanced CT (CECT), which employs contrast agents to vividly delineate the vasculature for detecting pathologies like aneurysms and stenoses, and non-contrast CT (NCCT). The latter is essential for visualizing specific conditions, such as atherosclerotic plaques, and serves as an alternative for patients with contraindications to contrast media, most notably renal insufficiency.

⋆ Corresponding author: lin.yao@nih.gov

Despite significant progress in automatic abdominal vessel segmentation [6, 7, 12], incomplete segmentation remains a persistent challenge. This issue persists even in powerful models such as TotalSegmentator (TS) [12], which segments 104 anatomic structures, including the aorta and iliac arteries, and is trained on 1,000 diverse CT scans. These methods often yield fragmented vessels with discontinuities, termed interruptions, in both NCCT and CECT images. Such errors stem from complex vascular morphology, surrounding anatomical structures, and imaging artifacts, and are particularly pronounced in NCCT images, where low vessel-to-background contrast obscures vessel boundaries.

Existing methods for correcting interruptions fall into two categories. Rule-based methods reconnect vessels via handcrafted post-processing. For example, Yao et al. constructed a centerline graph to identify interrupted regions and applied Dijkstra's algorithm to determine the minimal path on local CT images, completing the interruptions through region growing [15, 14]. However, these methods struggle with tortuous vascular topology and imaging noise. Learning-based methods train 3D CNN models [3] to restore missing segments or use topology-aware loss functions [9], but require large amounts of labeled training data, which is a critical bottleneck for NCCT images, where the absence of contrast agents makes annotation both difficult and unreliable. In contrast, CECT images offer clearer vascular visibility and are more amenable to annotation, making them a natural source of supervision. Our empirical observation confirms this disparity: TS produces substantially more complete segmentations on CECT than on paired NCCT images. This motivates a key question: can we leverage CECT annotations to supervise vessel completion in both NCCT and CECT images, thereby avoiding additional manual NCCT annotation, which is costly and challenging?

To address this, we draw on recent advances in 3D point cloud completion [2, 11, 18], which restore missing geometric structures from partial inputs. Given the tree-like tubular morphology of blood vessels, such methods adapt naturally to vessel completion regardless of imaging protocol. Concretely, we use TS as an off-the-shelf tool to obtain initial segmentation masks of the aorta and iliac arteries for both CECT and NCCT images, then train a vessel completion model supervised exclusively by CECT annotations to repair interruptions in both protocols, without requiring any additional manual NCCT annotation.

In this paper, we propose a 3D **Vess**el **Com**pletion **Net**work (**VessComNet**) designed to address the aforementioned challenges. Our key contributions are:

- **Cross-protocol training**: A strategy that leverages CECT annotations, which are more amenable to accurate labeling, to train a unified model for vessel completion in both CECT and challenging NCCT images, without requiring additional manual NCCT annotation.
- **Topology-aware interruption synthesis**: A data augmentation technique that generates diverse, anatomically realistic interruptions modeled on typical segmentation failures, improving model robustness and generalization.

– **Geometry-aware architecture**: A centerline-guided vessel completion network that explicitly preserves topological connectivity and produces structurally plausible vessel reconstructions.

We validated our approach through a comprehensive evaluation on three distinct datasets: a primary paired NCCT-CECT dataset, and two external test datasets composed of NCCT-only and CECT-only images. The results demonstrate that VessComNet outperforms baseline methods by producing more complete and topologically accurate vessel masks.

2 Methods

2.1 Problem Formulation

Given an incomplete vessel segmentation mask M_{init}, our goal is to generate a completed, topologically consistent vessel mask M by formulating the task as point cloud completion. Specifically, from M_{init} and its centerline C_{init}, we predict two point clouds: the missing surface $\hat{P}$ and the missing centerline $\hat{C}$. Explicitly predicting $\hat{C}$ is crucial, as it encourages the model to capture the vessel's global trajectory and topological backbone, thereby regularizing the surface prediction $\hat{P}$ to remain anatomically plausible. The final mask is constructed as $M = M_{\text{init}} \cup \text{voxelize}(\hat{P})$. By defining the problem purely on geometric masks, the method naturally generalizes across NCCT and CECT segmentations.

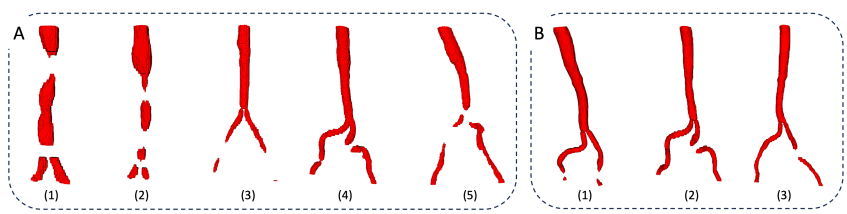

Fig. 1: Typical interruption patterns from TS segmentations, including at straight (A1-A3, B1, B3)/tortuous (A4, A5, B2) mid-vessel segments, bifurcations (A1, A2, A5), and vessel endings (A3). (A) Severe interruptions common in NCCT. (B) Less frequent but persistent incompleteness in CECT.

2.2 Topology-aware Interruption Synthesis

To improve model robustness and generalization, we introduce a topology-aware interruption synthesis technique that generates diverse and anatomically realistic interruptions for data augmentation. Our approach is guided by an analysis of segmentation-induced interruptions observed in TotalSegmentator (TS) outputs from both NCCT and CECT images. As illustrated in Fig. 1, these observed interruptions are not random; they exhibit distinct patterns. Notably, interruptions in NCCT scans are frequent and severe, even affecting large-diameter vessels, while those in CECT are predominantly confined to tortuous regions.

To systematically replicate these observed failure patterns, we first construct a topology-aware vascular graph [14] from a ground-truth CECT mask. We then analyze this graph to classify anatomical features based on their topological and geometric properties: bifurcations are identified via node degree, and curvature analysis distinguishes straight from tortuous segments. Finally, synthetic interruptions are generated by randomly sampling these classified subgraphs and excising the corresponding regions from the vessel mask. Training on this augmented dataset, combining both synthetic and segmentation-induced interruptions, equips our model to robustly complete vascular structures across both NCCT and CECT segmentations.

2.3 Geometry-Aware Vessel Completion

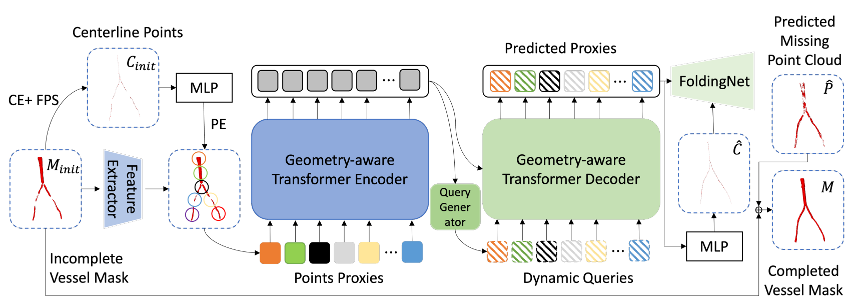

Fig. 2: Framework of the proposed VessComNet. CE: Centerline Extraction. FPS: Farthest Point Sampling. PE: Position Encoding.

Our 3D vessel completion network adapts PoinTr [16] with three vessel-specific modifications, as illustrated in Fig. 2: (1) a centerline-guided input representation that injects topological priors into local surface features, (2) a hierarchical decoder that first restores the centerline and then generates the surface point cloud conditioned on it, and (3) a composite loss function that jointly supervises surface geometry, centerline topology, and their mutual alignment.

Input Representation. The encoder input is constructed by fusing local surface features with global topological information from the vessel centerline. Surface points sampled from M_{init} are processed by a feature extractor to yield a set of permutation-invariant local feature vectors. In parallel, the partial centerline C_{init} is extracted, sampled via farthest point sampling (FPS) method [8], and embedded through an MLP to produce a sequence of centerline embeddings encoding the global vessel trajectory. Each local surface feature is then augmented with its nearest centerline embedding, injecting positional awareness along the vessel's topological backbone. The resulting enriched feature sequence forms the point proxies passed to the Transformer encoder.

Hierarchical Completion Network. The geometry-aware Transformer encoder-decoder processes the input proxies to produce a set of predicted proxies, which serve as a shared latent representation of the missing vessel geometry. These proxies are decoded in a hierarchical manner: an MLP head first recovers the missing centerline $\hat{\mathcal{C}}$, reconstructing the vessel's topological backbone. A FoldingNet decoder [13] then generates the missing surface point cloud $\hat{\mathcal{P}}$, conditioned on both the predicted proxies and the restored centerline $\hat{\mathcal{C}}$. By grounding surface generation in an explicit geometric scaffold, this hierarchical design encourages the completed vessel to maintain an anatomically plausible trajectory. The final completed vessel mask is obtained as $M = M_{\text{init}} \cup \text{voxelize}(\hat{\mathcal{P}})$.

Loss Function. The network is optimized with an objective that jointly supervises surface geometry, centerline topology, and their geometric consistency:

$$L_{\text{total}} = L_{\text{CD}}(\hat{P}, P_{gt}) + \lambda_1 L_{cl} + \lambda_2 L_{\text{cons}}, \tag{1}$$

where $\hat{P}, \hat{C}$ are the predicted missing surface and centerline point clouds, P_{gt}, C_{gt} their ground truths, and L_{CD} denotes the Chamfer distance, following PoinTr. The first two terms supervise completion, $L_{cl} = L_{\text{CD}}(\hat{C}, C_{gt})$; the third enforces the medial-axis property by driving each centerline node to the centroid of its local cross-section, $L_{\text{cons}} = \frac{1}{|\mathcal{I}|} \sum_{i \in \mathcal{I}} \left\| \hat{c}_i - \frac{1}{|S_i|} \sum_{p \in S_i} p \right\|_2^2$, with $S_i = \{p \in \hat{P} : i = \arg\min_j \|p - \hat{c}_j\|_2\}$ denoting the surface points assigned to node $\hat{c}_i$ by nearest-neighbor search, and $\mathcal{I} = \{i : |S_i| > 0\}$ denoting the set of centerline nodes with nonempty assignments. Nodes with empty assignments are excluded from L_{cons} and remain supervised by L_{cl}. This couples the two representations into a consistent vascular geometry; λ_1, λ_2 weight the last two terms.

3 Experiments and Results

3.1 Experimental Setup

Experiments are conducted on three datasets (Table 1). Training annotations were available only for the CECT scans in the Renal Donors cohort. For evaluation, a reference vessel mask was prepared for every test scan and was used exclusively for testing. Initial masks generated by TS were manually refined using ITK-SNAP [17] by two clinicians, each with more than three years of clinical experience. Refinement was performed in axial, coronal, and sagittal views to ensure anatomical plausibility and topological continuity. The check mark in the "Training Annotation" column of Table 1 therefore indicates the availability of annotations for training.

Renal Donors dataset This primary dataset contains paired NCCT and CECT volumes of the aorta and iliac arteries. The data were split at the subject level into 50 training, 13 validation, and 17 test subjects. Paired NCCT

Table 1: Overview of datasets and training configurations. The model is trained exclusively on the Renal Donors dataset and evaluated on all three datasets.

Dataset	Imaging Protocol	Scans	Train	Val	Test	Training Annotation
Renal Donors	NCCT	80	50	13	17	–
	CECT	80	50	13	17	✓
Vasculitis	NCCT	66	–	–	66	–
Urography	CECT	23	–	–	23	–

and CECT scans from the same subject, together with all derived samples and synthetic interruptions, were retained in the same split. Only CECT annotations are used for supervision. When paired NCCT images are available, they are registered to CECT space using ANTs [1], and the intersection between the TS segmentation and the CECT annotation mask is used as NCCT input in training, introducing segmentation-induced interruptions. However, paired data is not required: the model can be trained solely on synthetic interruptions generated from CECT annotations, without NCCT data. At inference, the model operates only on TS segmentation masks, without requiring paired scans. The training set is augmented with 1000 synthetic interruptions (20 per case).

External Test Datasets. The Vasculitis cohort initially comprised 74 NCCT scans covering the aorta and iliac arteries, of which 8 were excluded due to poor image quality, leaving 66 scans for evaluation. The Urography dataset comprised 23 scans and offers a distinct challenge, as its CECT images enhance the urinary system rather than the arteries seen in the Renal Donors' CECTs.

Evaluation Metrics. We evaluate segmentation quality using DSC and HD95, ASD for surface accuracy, and clDice [9] and Betti Error [4] for topological connectivity. The latter two metrics directly reflect the clinical requirement for continuous, uninterrupted vessel structures.

Implementation Details. VessComNet is implemented in PyTorch and trained on an NVIDIA A100 GPU with AdamW [5] (initial learning rate 5×10^{-4}, decayed by 0.9 every 20 epochs) for 300 epochs with batch size 32. BPR [10] standardizes the field of view to the aorta and iliac arteries. Surface and centerline point clouds are sampled via FPS to 16384 and 512 points, with inputs at half these sizes (8192 and 256), following the standard partial-to-complete setup [16]. The encoder produces G=256 proxies (k=8); the decoder predicts G'=256 missing proxies, each expanded by FoldingNet into S=32 points (8192 total). We set λ_1=1.0 and λ_2=0.1, warming up λ_2 after 30 epochs to stabilize the nearest-neighbor assignment. At inference, $\hat{\mathcal{P}}$ is voxelized and merged with M_{init}, collapsing duplicates, to produce the final mask M.

3.2 Quantitative Results

We compare VessComNet against two baselines in Table 2: TS [12], which provides the initial segmentation, and a rule-based method [14] that reconnects interruptions via centerline-graph-guided Dijkstra path completion. Connectivity-aware segmentation models (e.g., clDice-trained nnU-Net) are not included,

Table 2: Vessel completion performance across three datasets. TS and Rule-based serve as baseline methods. All values are reported as mean ± standard deviation; DSC and clDice are in %, HD95 and ASD are in mm, and Betti Error is unitless.

Datasets	Methods	DSC ↑	clDice ↑	HD95 ↓	ASD ↓	Betti Error ↓
Renal Donors (NCCT)	TS	80.9 ± 13.1	85.7 ± 9.7	8.2 ± 6.7	1.2 ± 0.8	2.643 ± 0.842
	Rule-based	82.4 ± 11.1	83.6 ± 8.9	6.3 ± 6.0	1.1 ± 0.6	**0.500 ± 0.519**
	VessComNet^{Seg}	84.1 ± 12.5	85.2 ± 11.7	6.0 ± 4.4	1.3 ± 0.8	1.412 ± 1.017
	VessComNet^{Syn}	90.6 ± 13.1	91.3 ± 10.9	4.1 ± 1.9	1.0 ± 0.7	0.647 ± 0.429
	VessComNet$^{Seg+Syn}$	**91.9 ± 6.1**	**93.2 ± 8.7**	**3.9 ± 1.2**	**0.7 ± 0.5**	0.588 ± 0.242
Renal Donors (CECT)	TS	93.2 ± 9.5	96.3 ± 7.8	1.9 ± 0.8	0.5 ± 0.2	0.294 ± 0.469
	Rule-based	94.1 ± 6.7	95.7 ± 7.3	1.4 ± 0.5	0.3 ± 0.2	0.286 ± 0.166
	VessComNet^{Seg}	93.4 ± 11.7	95.2 ± 8.1	1.6 ± 0.7	0.5 ± 0.2	0.235 ± 0.437
	VessComNet^{Syn}	95.8 ± 9.2	97.3 ± 3.2	1.0 ± 0.6	0.3 ± 0.2	0.118 ± 0.332
	VessComNet$^{Seg+Syn}$	**97.1 ± 2.5**	**99.5 ± 0.8**	**0.6 ± 1.0**	**0.1 ± 0.1**	**0.059 ± 0.243**
Vasculitis (NCCT)	TS	81.4 ± 11.4	83.4 ± 7.9	8.4 ± 4.7	2.4 ± 3.4	2.702 ± 1.889
	Rule-based	90.3 ± 16.8	82.8 ± 13.1	6.2 ± 2.6	0.8 ± 1.5	0.984 ± 1.293
	VessComNet^{Seg}	87.4 ± 19.5	89.4 ± 21.7	4.2 ± 2.1	1.0 ± 0.4	1.328 ± 1.216
	VessComNet^{Syn}	90.6 ± 16.4	91.7 ± 8.8	3.0 ± 1.9	1.0 ± 0.6	0.637 ± 1.027
	VessComNet$^{Seg+Syn}$	**93.1 ± 7.6**	**92.1 ± 6.3**	**2.6 ± 1.8**	**0.8 ± 0.7**	**0.482 ± 1.164**
Urography (CECT)	TS	94.1 ± 2.5	95.3 ± 3.4	4.4 ± 4.7	0.5 ± 0.3	1.478 ± 1.620
	Rule-based	93.9 ± 2.9	94.0 ± 5.4	4.0 ± 4.2	0.5 ± 0.3	0.739 ± 1.514
	VessComNet^{Seg}	94.3 ± 4.7	95.8 ± 7.1	2.0 ± 1.3	0.3 ± 0.2	0.957 ± 1.424
	VessComNet^{Syn}	95.7 ± 3.9	96.3 ± 5.7	**1.7 ± 1.0**	**0.2 ± 0.1**	0.609 ± 1.192
	VessComNet$^{Seg+Syn}$	**96.1 ± 2.3**	**97.9 ± 1.9**	2.9 ± 3.7	0.3 ± 0.2	**0.478 ± 0.994**

as they require manual NCCT annotations. We evaluate three training configurations: VessComNet^{Syn} uses synthetic interruptions, VessComNet^{Seg} uses segmentation-induced interruptions, and VessComNet$^{Seg+Syn}$ uses both interruption types. We also conduct an ablation study on centerline supervision.

Renal Donors Dataset. On CECT, where contrast renders the vasculature clearly, all methods attain strong baselines (93.2% and 94.1% DSC for TS and rule-based). VessComNet$^{Seg+Syn}$ further reaches 97.1% DSC and 99.5% clDice while lowering Betti Error to 0.059 (vs. 0.294 and 0.286), yielding near-complete and topologically faithful reconstructions. The high fidelity on CECT allows the completed vessels to serve as reliable supervision for more challenging NCCT.

On the more challenging NCCT set, rule-based increases DSC (82.4% vs. 80.9%) but reduces clDice (83.6% vs. 85.7%). In contrast, VessComNet$^{Seg+Syn}$ achieves 91.9% DSC and 93.2% clDice, reduces Betti Error from 2.643 for TS to 0.588, although the rule-based method achieves a lower value of 0.500. The consistent improvements highlight the effectiveness of learned geometric completion, which is most pronounced on this more interrupted NCCT.

External Test Datasets. On Vasculitis (NCCT), VessComNet$^{Seg+Syn}$ improves DSC from 81.4% to 93.1% and clDice from 83.4% to 92.1%, reducing Betti Error to 0.482. Rule-based improves DSC (90.3%) but remains limited in connectivity (82.8% clDice). On Urography (CECT), in terms of DSC, rule-based does not outperform TS (93.9% vs. 94.1%), whereas VessComNet$^{Seg+Syn}$ achieves 96.1% DSC and 97.9% clDice with the lowest Betti Error (0.478). These results demonstrate consistent connectivity gains and strong cross-dataset generalization.

Effect of Interruption Synthesis. Across datasets, VessComNet^{Syn} generally outperforms VessComNet^{Seg}, while their combination (VessComNet$^{Seg+Syn}$) achieves the best DSC and clDice and the lowest Betti Error in most settings, suggesting that both interruption types are beneficial.

Table 3: Ablation Studies on Renal Donors NCCT Test Dataset.

L_{cl}	L_{cons}	DSC↑	clDice↑	Betti↓
✗	✗	81.3	82.7	1.376
✓	✗	87.8	88.2	0.975
✓	✓	**91.9**	**93.2**	**0.588**

Effect of Centerline Supervision. We ablate the two centerline-related losses on Renal Donors NCCT (Table 3). L_{cl} improves all metrics over the baseline, while L_{cons} further raises clDice and lowers the Betti Error. The larger gains on connectivity metrics confirm that centerline-guided completion losses enhance topological connectivity.

3.3 Qualitative Results

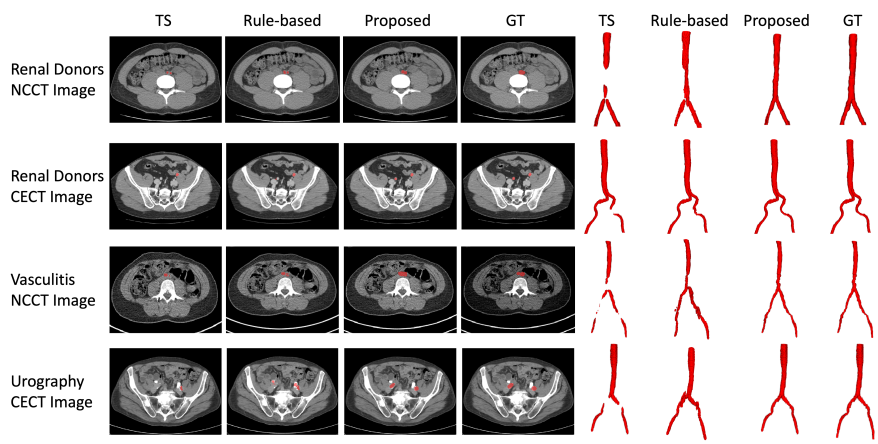

Fig. 3: Qualitative vessel completion results across three datasets. From left to right: TS, rule-based, VessComNet, and ground truth (GT). Left panels show axial slices; right panels show corresponding 3D visualizations.

Fig. 3 presents representative vessel completion results across three datasets. Columns 1-4 show axial slices of TS, rule-based, VessComNet, and ground truth, respectively, with corresponding 3D visualizations in Columns 5-8. For NCCT images (Rows 1 and 3), severe interruptions are observed along the aorta, bifurcations, and iliac branches. While the rule-based method reconnects some fragmented segments, it occasionally introduces spurious connections or artificial bridges between branches, and may leave residual disconnections in complex regions. These issues are more evident in the 3D renderings, where irregular trajectories and locally distorted topology can be observed. In contrast, VessComNet restores continuous and anatomically coherent vessels with smoother centerline trajectories, closely matching the ground truth and preserving bifurcation structure. For CECT images (Rows 2 and 4), interruptions are primarily located in tortuous segments. The rule-based approach sometimes produces incomplete reconnections or geometrically inconsistent bridges in highly curved regions. VessComNet, however, maintains both structural continuity and curvature consistency, yielding more plausible 3D reconstructions. Overall, the qualitative results indicate that heuristic reconnection may partially recover continuity but can introduce topological inconsistencies or residual gaps, whereas geometry-aware completion achieves more anatomically consistent vessel restoration.

4 Conclusion

We proposed VessComNet, a geometry-aware 3D vessel completion method to repair vessel interruptions in both NCCT and CECT segmentations. Notably, our solution enables NCCT vessel completion without requiring additional manual NCCT annotations. Our approach uses a topology-aware centerline vascular graph to synthesize interruptions, enhancing both the diversity and quantity of training data. Furthermore, by utilizing the high-level structure of the centerline to capture geometric information and incorporating centerline Chamfer loss, we effectively encourage the model to learn the correct topology, thereby improving vessel connectivity. Validated on the aorta and iliac arteries across three datasets, our method effectively completes interruptions in both NCCT and CECT. Although these vessels are simple, improving their continuity in NCCT is clinically important. Future work will extend this framework to more complex structures, like the cerebral and coronary arteries, and across imaging modalities.

Acknowledgments. This research was supported by the Intramural Research Program of the National Institutes of Health (NIH). This work utilized the computational resources of the NIH HPC Biowulf cluster (https://hpc.nih.gov).

Ethics Statement. The Renal Donors non-NIH dataset was anonymized prior to receipt by NIH and NIH IRB review was not required. Usage of the Vasculitis and Urography datasets was approved for retrospective research by the NIH IRB under Protocol #000037; the requirement for informed consent was waived.

Disclosure of Interests. Dr. Perry J. Pickhardt is an advisor to Bracco, Nanox, GE Healthcare, and ColoWatch. Dr. Ronald M. Summers received royalties for patents or software licenses from iCAD, Philips, and ScanMed. The remaining authors have no relevant financial or non-financial interests to disclose.

Disclaimer. This research was supported in part by the Intramural Research Program of the National Institutes of Health (NIH). The contributions of the NIH authors are considered Works of the United States Government. The findings and conclusions presented in this paper are those of the authors and do not necessarily reflect the views of the NIH or the U.S. Department of Health and Human Services.

References

1. Avants, B.B., Tustison, N., Song, G., et al.: Advanced normalization tools (ants). Insight J **2**(365), 1–35 (2009)
2. Fei, B., Yang, W., Chen, W.M., Li, Z., Li, Y., Ma, T., Hu, X., Ma, L.: Comprehensive review of deep learning-based 3d point cloud completion processing and analysis. IEEE Transactions on Intelligent Transportation Systems **23**(12), 22862–22883 (2022)
3. Fu, F., Wei, J., Zhang, M., Yu, F., Xiao, Y., Rong, D., Shan, Y., Li, Y., Zhao, C., Liao, F., et al.: Rapid vessel segmentation and reconstruction of head and neck angiograms using 3d convolutional neural network. Nature Communications **11**(1), 4829 (2020)
4. Hu, X., Li, F., Samaras, D., Chen, C.: Topology-preserving deep image segmentation. Advances in Neural Information Processing Systems **32** (2019)
5. Loshchilov, I., Hutter, F.: Decoupled weight decay regularization. In: International Conference on Learning Representations (ICLR) (2019)
6. Moccia, S., De Momi, E., El Hadji, S., Mattos, L.S.: Blood vessel segmentation algorithms—review of methods, datasets and evaluation metrics. Computer Methods and Programs in Biomedicine **158**, 71–91 (2018)
7. Oda, M., Roth, H.R., Kitasaka, T., Misawa, K., Fujiwara, M., Mori, K.: Abdominal artery segmentation method from ct volumes using fully convolutional neural network. International Journal of Computer Assisted Radiology and Surgery **14**, 2069–2081 (2019)
8. Qi, C.R., Su, H., Mo, K., Guibas, L.J.: Pointnet: Deep learning on point sets for 3d classification and segmentation. In: Proceedings of the IEEE Conference on Computer Vision and Pattern Recognition. pp. 652–660 (2017)
9. Shit, S., Paetzold, J.C., Sekuboyina, A., Ezhov, I., Unger, A., Zhylka, A., Pluim, J.P., Bauer, U., Menze, B.H.: cldice-a novel topology-preserving loss function for tubular structure segmentation. In: Proceedings of the IEEE/CVF Conference on Computer Vision and Pattern Recognition. pp. 16560–16569 (2021)
10. Tang, Y., Gao, R., Han, S., Chen, Y., Gao, D., Nath, V., Bermudez, C., Savona, M.R., Bao, S., Lyu, I., et al.: Body part regression with self-supervision. IEEE Transactions on Medical Imaging **40**(5), 1499–1507 (2021)
11. Tesema, K.W., Hill, L., Jones, M.W., Ahmad, M.I., Tam, G.K.: Point cloud completion: A survey. IEEE Transactions on Visualization and Computer Graphics (2023)
12. Wasserthal, J., Breit, H.C., Meyer, M.T., Pradella, M., Hinck, D., Sauter, A.W., Heye, T., Boll, D.T., Cyriac, J., Yang, S., et al.: Totalsegmentator: Robust segmentation of 104 anatomic structures in ct images. Radiology: Artificial Intelligence **5**(5) (2023)
13. Yang, Y., Feng, C., Shen, Y., Tian, D.: Foldingnet: Point cloud auto-encoder via deep grid deformation. In: 2018 IEEE/CVF conference on computer vision and pattern recognition. pp. 206–215. IEEE (2018)
14. Yao, L., Shi, F., Wang, S., Zhang, X., Xue, Z., Cao, X., Zhan, Y., Chen, L., Chen, Y., Song, B., et al.: Tag-net: Topology-aware graph network for centerline-based vessel labeling. IEEE Transactions on Medical Imaging **42**(11), 3155–3166 (2023)
15. Yao, L., Xue, Z., Zhan, Y., Chen, L., Chen, Y., Song, B., Wang, Q., Shi, F., Shen, D.: Tag-net: Topology-aware graph network for vessel labeling. In: MICCAI Workshop on Imaging Systems for GI Endoscopy. pp. 108–117. Springer (2022)

16. Yu, X., Rao, Y., Wang, Z., Liu, Z., Lu, J., Zhou, J.: Pointr: Diverse point cloud completion with geometry-aware transformers. In: Proceedings of the IEEE/CVF international conference on computer vision. pp. 12498–12507 (2021)
17. Yushkevich, P.A., Piven, J., Hazlett, H.C., Smith, R.G., Ho, S., Gee, J.C., Gerig, G.: User-guided 3d active contour segmentation of anatomical structures: significantly improved efficiency and reliability. Neuroimage **31**(3), 1116–1128 (2006)
18. Zhuang, Z., Zhi, Z., Han, T., Chen, Y., Chen, J., Wang, C., Cheng, M., Zhang, X., Qin, N., Ma, L.: A survey of point cloud completion. IEEE Journal of Selected Topics in Applied Earth Observations and Remote Sensing (2024)